

## Local Control of Single Atom Magnetocrystalline Anisotropy

B. Bryant, A. Spinelli, J. J. T. Wagenaar, M. Gerrits, and A. F. Otte\*

*Department of Quantum Nanoscience, Kavli Institute of Nanoscience, Delft University of Technology,  
Lorentzweg 1, 2628 CJ Delft, The Netherlands*

(Received 8 May 2013; published 17 September 2013)

Individual Fe atoms on a Cu<sub>2</sub>N/Cu(100) surface exhibit strong magnetic anisotropy due to the crystal field. We show that we can controllably enhance or reduce this anisotropy by adjusting the relative position of a second nearby Fe atom, with atomic precision, in a low-temperature scanning tunneling microscope. Local inelastic electron tunneling spectroscopy, combined with a qualitative first-principles model, reveal that the change in uniaxial anisotropy is driven by local strain due to the presence of the second Fe atom.

DOI: [10.1103/PhysRevLett.111.127203](https://doi.org/10.1103/PhysRevLett.111.127203)

PACS numbers: 75.75.-c, 75.10.Dg, 75.30.Gw, 81.16.Ta

The manner in which individual magnetic atoms interact with their environment ultimately determines the macroscopic magnetic properties of materials. Recent experimental advances such as the ability to probe and manipulate individual magnetic atoms using scanning tunneling microscopy (STM) [1–3] make it possible to investigate these interactions in detail. In general, two competing processes can be identified, which both influence the preferred orientation of atomic spins. On one hand, magnetic anisotropy due to spin-orbit coupling and the local crystal field favors certain axes for magnetization over others [4–7]. On the other hand, neighboring spins can be subject to spin coupling due to, e.g., superexchange [8,9] or Ruderman-Kittel-Kasuya-Yosida interaction [10–12], leading to either ferromagnetic or antiferromagnetic alignment of the spins.

An interesting situation arises when spin coupling and magnetic anisotropy energies are comparable [13–15]. Recently, it was shown that placing only a few atoms in this type of configuration results in remarkably stable magnetic structures [15,16]. Understanding the physical mechanisms underlying this sudden emergence of magnetic stability is of great importance for the development of nanoscale data storage solutions.

In this Letter, we demonstrate that single atom magnetic anisotropy may be tuned by atomically precise relative positioning of two magnetic atoms. Using atom manipulation in a low-temperature STM, we construct on a Cu<sub>2</sub>N substrate a set of three geometrically distinct Fe dimers. From inelastic tunneling spectroscopy on each dimer, we infer that the anisotropy of the Fe atom varies according to the precise positioning of its neighbor: the uniaxial anisotropy parameter  $D$  may be either enhanced or reduced by values up to 20%. Further, via a qualitative first-principles model, we can attribute these changes in anisotropy to variation in the N–Fe–N angle, driven by local strain due to the presence of the second Fe atom.

Atomic structure and STM topographic images of each of the three types of dimers are shown in Figs. 1(a)–1(c). The dimers all have the same bond length within the Cu<sub>2</sub>N surface network. We classify the dimers according to the

number of unit cells separating the two atoms in each symmetry direction. For example, the dimer shown in Fig. 1(b) will be referred to as  $\{3/2, 1/2\}$ . Each Fe atom on Cu<sub>2</sub>N has a magnetic easy axis which is oriented toward the neighboring N atoms ( $D < 0$ ) [5]. As such, the atoms in the  $\{3/2, 1/2\}$  dimer have their easy axes oriented perpendicular to each other. The atoms in the  $\{2, 0\}$  dimer [Fig. 1(a)] have parallel easy axes. This structure is identical to the atomic arrangement described previously by Loth *et al.* [15]. Finally, the atoms in the  $\{1, 1\}$  dimer [Fig. 1(c)] have parallel but laterally offset easy axes.

We performed inelastic electron tunneling spectroscopy (IETS) measurements [1] at 330 mK on each of the atoms in our Fe dimers, in various magnetic fields [Figs. 1(d)–1(f) and S1]. In the resulting differential conductance spectra, spin excitations appear as distinct steps at voltages corresponding to the excitation energies. Excitations measured on our dimers have significantly shifted compared to those found on isolated Fe atoms on Cu<sub>2</sub>N [5]. In the following, we demonstrate how these energy shifts can be accounted for in terms of modifications to the local crystal field due to local strain and spin coupling. Note that the two atoms of the  $\{3/2, 1/2\}$  dimer show IETS spectra that differ from one another [Fig. 1(b)]: assuming isotropic spin coupling, this difference can only be accounted for by variation in  $D$ .

We modeled the observed excitation energies using a Heisenberg Hamiltonian [17]

$$\hat{\mathcal{H}} = \sum_{i=A,B} \hat{\mathcal{H}}^{(i)} + J \hat{\mathbf{S}}^{(A)} \cdot \hat{\mathbf{S}}^{(B)}, \quad (1)$$

which couples the spins  $\mathbf{S}^{(i)}$  of atoms  $A$  and  $B$  in the dimer through a Heisenberg coupling parameter  $J$ . The single spin anisotropy Hamiltonian  $\hat{\mathcal{H}}^{(i)}$  describes for each spin the magnetic anisotropy and the Zeeman effect due to an external magnetic field  $\mathbf{B}$  ( $\mu_B$  being the Bohr magneton):

$$\begin{aligned} \hat{\mathcal{H}}^{(i)} = & D^{(i)} \hat{S}_z^{2(i)} + E^{(i)} (\hat{S}_x^{2(i)} - \hat{S}_y^{2(i)}) \\ & - \mu_B \sum_{\mu=x,y,z} g_{\mu}^{(i)} B_{\mu} \hat{S}_{\mu}^{(i)}. \end{aligned} \quad (2)$$

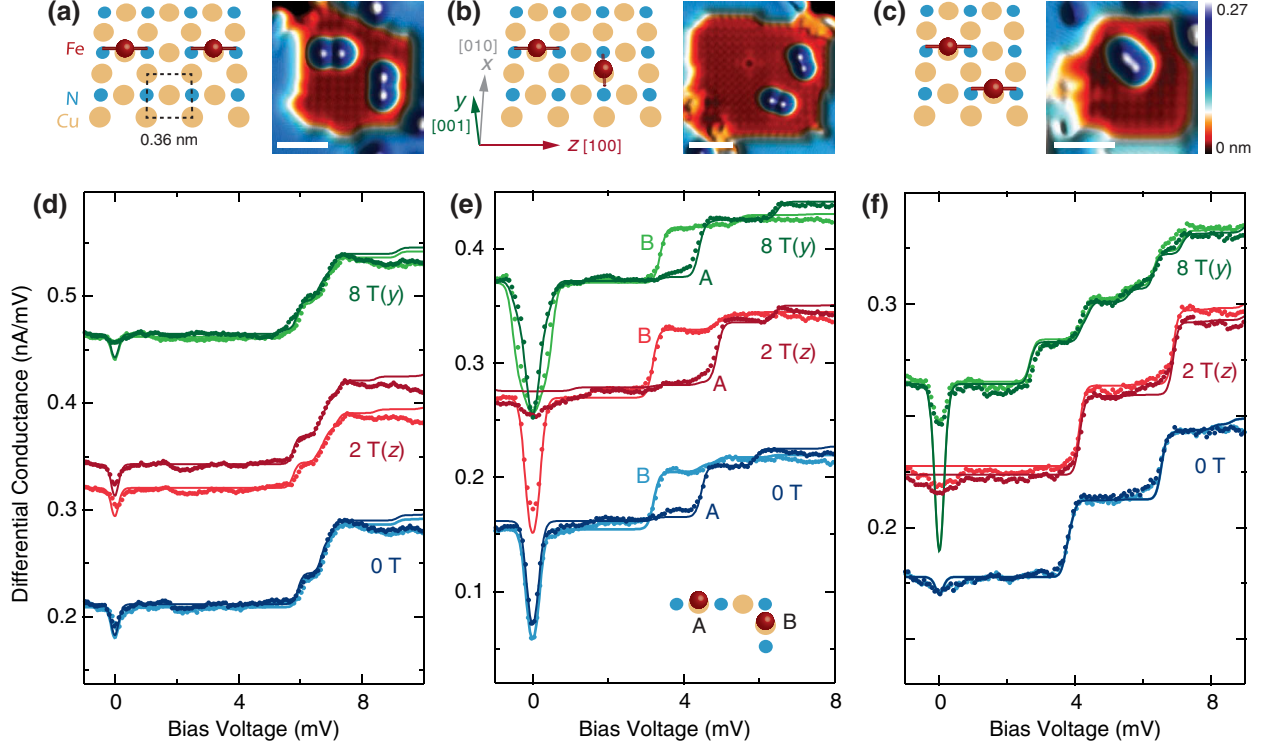


FIG. 1 (color online). (a–c) Diagrams and STM topographic images for (a)  $\{2, 0\}$  dimer, (b)  $\{3/2, 1/2\}$  dimer, and (c)  $\{1, 1\}$  dimer. Magnetic easy axes for Fe atoms are indicated by red lines: the  $\text{Cu}_2\text{N}$  unit cell is shown in (a). Topographic scale bars correspond to 2 nm. (d–f) Measured IETS spectra (dots) and corresponding simulated spectra (lines) on all three types of dimers, for zero magnetic field and magnetic fields applied in the  $z$  and  $y$  directions. At-field spectra offset for clarity; the STM temperature is 330 mK. In (e), atoms  $A$  and  $B$  are distinguished; in (d) and (f), the atoms of the dimer are essentially identical, but both sets of spectra are presented for comparative purposes. The discrepancy between measured and simulated spectra near zero bias in (f) for 8 T( $y$ ) can be accounted for by assuming a  $\sim 2^\circ$  misalignment of the magnetic field to the  $y$  axis.

Here, the  $z$  axis is defined parallel to the in-plane easy axis of the Fe atom. The anisotropy parameters  $D^{(i)}$  and  $E^{(i)}$  as well as the  $g$  tensor  $g_\mu^{(i)}$  follow from second order perturbation treatment of the spin-orbit coupling  $\lambda \mathbf{L}^{(i)} \cdot \mathbf{S}^{(i)}$  [18]:

$$D^{(i)} = -\frac{\lambda^2}{2}(2\Lambda_{zz}^{(i)} - \Lambda_{xx}^{(i)} - \Lambda_{yy}^{(i)}), \quad (3)$$

$$E^{(i)} = -\frac{\lambda^2}{2}(\Lambda_{xx}^{(i)} - \Lambda_{yy}^{(i)}), \quad (4)$$

$$g_\mu^{(i)} = 2(1 - \lambda\Lambda_{\mu\mu}^{(i)}). \quad (5)$$

In these expressions, the parameters  $\Lambda_{\mu\mu}^{(i)}$  represent the degree of unquenched orbital momentum along the  $\mu$  direction (where  $\mu = x, y, z$ ). These are defined as

$$\Lambda_{\mu\mu}^{(i)} \equiv \sum_n \frac{|\langle \psi_0 | \hat{L}_\mu^{(i)} | \psi_n \rangle|^2}{E_n - E_0}, \quad (6)$$


where the sum runs over all  $n$  orbital excited states  $\psi_n$ , which have energies  $E_n$  [18,19]. As such, the energy difference in the denominator directly relates to the crystal field splitting of the orbitals. Unlike recently argued [20],

the anisotropy Hamiltonian (2) should be projected only onto the basis of spin states (using  $S = 2$  for Fe), not the orbital states, as this projection is already incorporated in the  $\Lambda_{\mu\mu}^{(i)}$  parameters. The negative value of the spin-orbit constant  $\lambda = -12.4$  meV [18] agrees with previously observed  $g$  values  $g > 2$  [5,13].

Using the total Heisenberg Hamiltonian (1), we generated simulated IETS spectra, as described in Refs. [5,21,22]. As discussed below,  $\Lambda_{zz}$  is much more sensitive to local strain than  $\Lambda_{xx}$  and  $\Lambda_{yy}$ . Therefore, the only parameters that were allowed to vary between atoms were  $\Lambda_{zz}$  and  $J$ , so the transverse anisotropy parameter  $E$  was not changed from its isolated-atom value 0.31 meV [5]. By carefully fitting simulated spectra to the measured spectra on each atom for all magnetic field directions, as shown in Figs. 1(d)–1(f) and Fig. S1, we find values for  $J$ ,  $\Lambda_{zz}$ , and  $D$  for all three dimers. These values are summarized in Table I.

Close inspection of the obtained parameter values reveals that the magnitude of the uniaxial anisotropy parameter  $|D|$  has increased compared to its isolated-atom value  $D = -1.55$  meV [5] for both atoms in the  $\{2, 0\}$  dimer and for atom  $A$  in the  $\{3/2, 1/2\}$  dimer. In contrast, it has decreased for atom  $B$  in the  $\{3/2, 1/2\}$  dimer and for

TABLE I. Values for  $J$ ,  $\Lambda_{zz}$ , and  $D$  (which follows from  $\Lambda_{zz}$ ) found for each atom in all three types of Fe dimer, studied by fitting measured IETS spectra with simulated spectra. Only in the case of the  $\{3/2, 1/2\}$  dimer are atoms  $A$  and  $B$  distinguishable. In the last row, for each atom, the anisotropy energy shift  $\Delta D$  with respect to the isolated-atom value  $D = -1.55$  meV is presented. For all atoms, we found  $\Lambda_{xx} = 0$  and  $\Lambda_{yy} = 4.0$  eV $^{-1}$ , giving  $E = 0.31$  meV. An identical constant of up to  $2$  eV $^{-1}$  can be added to all the  $\Lambda_{\mu\mu}$  values without visibly altering the simulated spectra. This constant has no influence on the values for  $J$ ,  $D$ , and  $E$ .

Dimer type			
	$\{2, 0\}$	$\{3/2, 1/2\}$	$\{1, 1\}$
$J$ (meV)	+0.70	A +0.20 B	-0.69
$\Lambda_{zz}$ (eV $^{-1}$ )	14.2	13.1 10.5	10.9
$D$ (meV)	-1.87	-1.70 -1.30	-1.37
$\Delta D$ (meV)	-0.32	-0.15 +0.25	+0.18

both atoms in the  $\{1, 1\}$  dimer. It appears, therefore, that for Fe atoms on  $\text{Cu}_2\text{N}$ , the magnitude of the uniaxial anisotropy increases when a second atom is placed along (or within one bond length of) its easy axis, and that it decreases for those atoms where the second atom is further away from the easy axis.

In order to explain the observed behavior qualitatively, we consider the immediate environment of the Fe atom, specifically its two nearest-neighbor N atoms, as shown in Fig. 2(a). According to previously published density functional theory (DFT) calculations, in the case of an isolated Fe atom on  $\text{Cu}_2\text{N}$ , the N atoms are situated slightly lower than the Fe atom [23]. The resulting crystal field has  $C_{2v}$  symmetry, which lifts all degeneracies between the five  $d$ -orbitals [25] [Fig. 2(b)]. In this situation, the expression (6) for  $\Lambda_{\mu\mu}$  reduces to matrix elements of  $\hat{L}_\mu$  in the basis of  $d$ -orbital states, many of which are zero [18,22]. Specifically, the unquenched orbital momentum along the  $z$  axis  $\Lambda_{zz}$  depends only on the energy difference  $E_1 - E_0$  between the  $d_{xy}$  and  $d_{x^2-y^2}$  orbitals [Fig. 2(b)] and is inversely proportional to this energy difference. This means that if the N-Fe-N angle  $\theta$  becomes closer to  $180^\circ$ ,  $E_1 - E_0$  tends to zero, and  $\Lambda_{zz}$  and therefore  $|D|$  rapidly increase. Likewise, if the angle becomes smaller,  $|D|$  decreases. In contrast,  $\Lambda_{xx}$  and  $\Lambda_{yy}$  (and therefore the transverse anisotropy  $E$ ) relate to the energy differences  $E_2 - E_0$  and  $E_3 - E_0$ , which remain finite in the limit  $\theta \rightarrow 180^\circ$  and therefore will depend much less dramatically on the bond angle.

Figures 2(c)–2(f) demonstrate how the observed variations in  $D$  in our dimers can be explained in terms of changes to the N-Fe-N angle, which follow from the previously known relaxation of Fe/ $\text{Cu}_2\text{N}$ . When an Fe atom is deposited on  $\text{Cu}_2\text{N}$ , the neighboring N atoms and

the next-nearest-neighbor Cu atoms are pulled upward and toward the Fe atom [5]. In the case of the  $\{2, 0\}$  dimer, we may expect that the central Cu atom will be raised even more, due to bonding to two Fe atoms, leading to an increased N-Fe-N angle [Fig. 2(d)] and hence increased

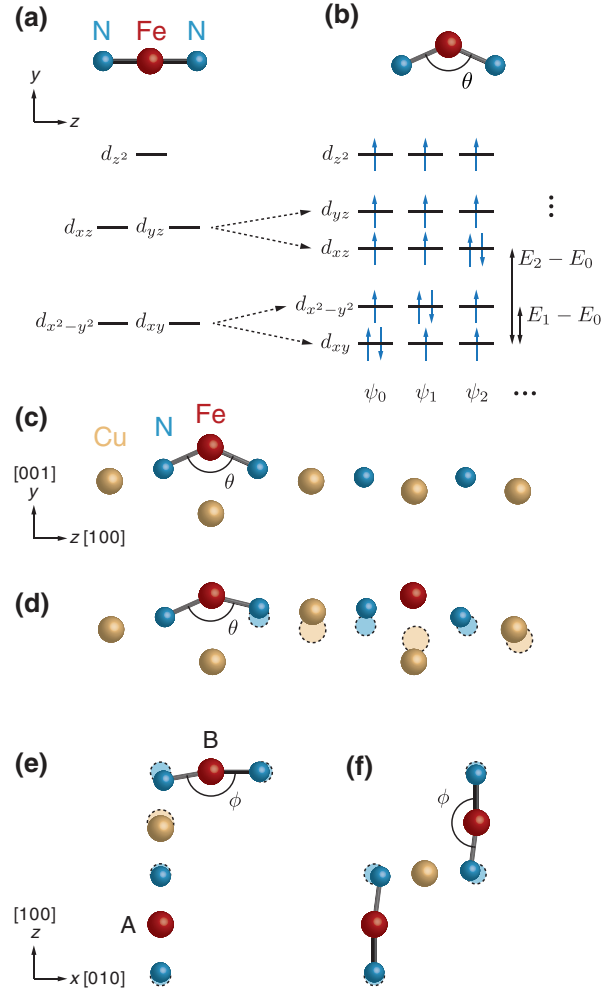


FIG. 2 (color online). (a) Splitting of  $d$ -orbital energies in a linear crystal field. (b) Splitting of  $d$ -orbital energies in a crystal field where the ligand-metal-ligand angle  $\theta$  is slightly smaller than  $180^\circ$ . The electron configurations for the orbital states  $\psi_n$  are shown. (c) Schematic of a single Fe adsorbed onto  $\text{Cu}_2\text{N}$ , after structure calculated using DFT [5]: a section in the  $yz$  plane along the Cu-N direction is shown. (d) Equivalent schematic section of the  $\{2, 0\}$  Fe dimer: dashed outlines show atom positions for the single Fe case. Since the central Cu atom is lifted due to bonding to two Fe atoms,  $\theta$  is larger (closer to  $180^\circ$ ) for the dimer than for a single Fe atom. (e) Schematic of a  $\{3/2, 1/2\}$  Fe dimer in the  $xz$  plane. For a single Fe atom adsorbed onto  $\text{Cu}_2\text{N}$ , the N-Fe-N angle in the  $xz$  plane  $\phi = 180^\circ$ : in the case of the  $\{3/2, 1/2\}$  dimer, the presence of Fe  $A$  compresses bond lengths along the Cu-N direction [as in (d)], so that for Fe  $B$ ,  $\phi < 180^\circ$ . Similarly, for the  $\{1, 1\}$  dimer (f), for both Fe atoms,  $\phi < 180^\circ$ . In (e) and (f), dashed outlines show the unperturbed  $\text{Cu}_2\text{N}$  lattice. Atomic displacements are only indicative and are not to scale.

$|D|$ . The same reasoning applies to atom  $A$  of the  $\{3/2, 1/2\}$  dimer. For atom  $B$  of this dimer, the situation is different. In this case, we expect the  $N$  atom to be pulled sideways due to the strain caused by atom  $A$ , as a result of which the  $N$ -Fe- $N$  angle in the horizontal plane decreases [Fig. 2(e)], leading to a decreased  $|D|$  value. A similar situation occurs for both atoms of the  $\{1, 1\}$  dimer [Fig. 2(f)]. It should be noted that we assume that the strain modifies only the crystal field of the Fe atom and that the spin moment and coupling to the electron bath are not changed from the single atom case. Evaluation of these parameters would require a full DFT treatment, which is beyond the scope of this study.

It is possible to estimate the orbital energy splittings based on the measured values of  $D$ ,  $E$ , and  $g_{\mu}$ . According to Eqs. (3) and (4), adding an identical offset to  $\Lambda_{xx}$ ,  $\Lambda_{yy}$ , and  $\Lambda_{zz}$  will not affect  $D$  or  $E$ , and hence a very high magnetic field would be necessary to separately define all the  $\Lambda_{\mu\mu}$ . However, by making fits to IETS data taken on an isolated Fe atom in magnetic fields up to 7 T in all three directions [5], we can constrain this offset to  $<2$  eV $^{-1}$ . Using median values for  $\Lambda_{zz}$  in Eq. (6), we find that  $E_1 - E_0 = 310 \pm 30$  meV for the isolated Fe atom and ranges from  $260 \pm 20$  meV for the atoms in the  $\{2, 0\}$  dimer to  $350 \pm 30$  meV for atom  $B$  of the  $\{3/2, 1/2\}$  dimer. The magnitude of these values compared to the spin-orbit constant  $\lambda = -12.4$  meV justifies our choice to treat spin-orbit coupling as a perturbation with respect to the crystal field.

Additional validation for our interpretation of strain-induced changes in anisotropy comes from studying variation between multiple instances of the  $\{3/2, 1/2\}$  dimer. Figure 3 shows IETS spectra taken on both atoms of 14 different instances of this dimer at zero magnetic field: for these dimers, we find  $D$  values varying from the mean by  $\pm 6\%$ . The anisotropy shifts are anticorrelated between atoms  $A$  and  $B$  (see the inset of Fig. 3). This suggests a variation in local *lattice* strain, applied to the whole dimer: if the local lattice is expanded, the strain induced by each Fe atom in the dimer on the other is reduced, and both Fe atoms'  $D$  values move closer to the isolated-atom value of  $D = -1.55$  meV [26]. Variation in spin excitation energies of  $\pm 5\%$  were previously observed for single Fe atoms on  $\text{Cu}_2\text{N}$  and were attributed changes in the local environment caused by strain in the  $\text{Cu}_2\text{N}$  islands [5,27].

In the current study, the simulated IETS spectra were produced using a purely isotropic Heisenberg coupling parameter  $J$ . This is in contrast with previous work on the  $\{2, 0\}$  dimer, in which only coupling between the  $z$  components of the spins was considered, giving  $J_z = +1.2$  meV [15]. In conjunction with increased values for  $|D|$ , we find a lower value  $J = +0.70$  meV for this dimer. In addition to the observed changes in  $D$ , Table I also indicates variation in the strength and sign of the coupling  $J$ , which changes from antiferromagnetic in the

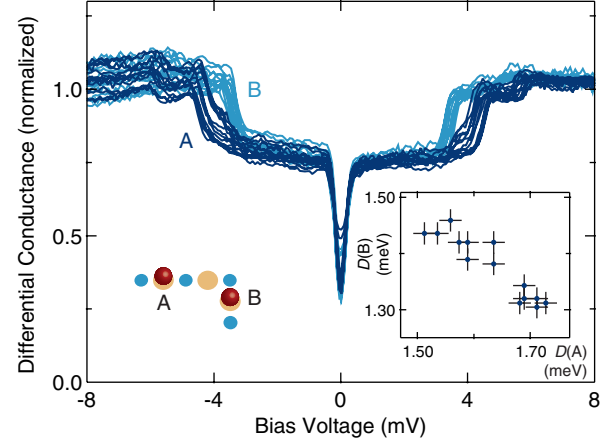


FIG. 3 (color online). IETS measurements performed on 14 different instances of the type  $\{3/2, 1/2\}$  dimer at 330 mK and zero magnetic field, showing a spread of the step positions for both atoms in the dimer. Spectra were collected at either 0.9 or 2 nA; no current dependence on the step position was observed. In the inset, the anisotropies of the two atoms of each dimer  $D^{(A)}$  and  $D^{(B)}$ , obtained by fitting the measured IETS spectra, are plotted against each other, indicating a strong anticorrelation between the two atoms (with Pearson correlation coefficient  $R = -0.93$ ). The error bars represent the fitting uncertainty for  $D$ .

$\{2, 0\}$  and  $\{3/2, 1/2\}$  dimers to ferromagnetic in the  $\{1, 1\}$  dimer. The change in sign of  $J$  is probably due to the distance dependence of the Ruderman-Kittel-Kasuya-Yosida interaction, although we cannot exclude potential influence from superexchange, as the total coupling is likely a combination of these two factors [28]. The ability to tune the sign of the interatomic magnetic coupling through atom manipulation will enable atomically engineered spin structures to be designed in which a broad range of magnetic phenomena is realized.

In summary, we have been able to control the magneto-crystalline anisotropy of a magnetic adatom embedded in a covalent surface network by carefully adjusting the position of a second nearby adatom. Strain due to the presence of this second adatom causes a slight change in the angle between the magnetic atom and its neighboring ligands. Using a qualitative first-principles model, we demonstrate that the magnetic anisotropy depends highly sensitively on this angle. We suggest that this strain-enhanced anisotropy may play a critical role in the reported magnetic stabilization of atomically assembled antiferromagnetic structures [15]. The ability to engineer magnetic anisotropy at the atomic scale will enable the creation of novel atomic-scale magnetic memory devices and low-dimensional spin lattices.

We thank J. Fernández-Rossier, C.F. Hirjibehedin, A.J. Heinrich, and G.A. Steele for discussions and R. Hoogerheide for technical support. This work was supported by the Dutch funding organizations FOM and NWO (VIDI) and by the Kavli Foundation. B. B. and A. S. contributed equally to this work.

\*a.f.otte@tudelft.nl

- [1] A. J. Heinrich, J. A. Gupta, C. P. Lutz, and D. M. Eigler, *Science* **306**, 466 (2004).
- [2] H. J. Lee, W. Ho, and M. Persson, *Phys. Rev. Lett.* **92**, 186802 (2004).
- [3] A. A. Khajetoorians, B. Chilian, J. Wiebe, S. Schuwalow, F. Lechermann, and R. Wiesendanger, *Nature (London)* **467**, 1084 (2010).
- [4] P. Gambardella, S. Rusponi, M. Veronese, S. S. Dhesi, C. Grazioli, A. Dallmeyer, I. Cabria, R. Zeller, P. H. Dederichs, K. Kern, C. Carbone, and H. Brune, *Science* **300**, 1130 (2003).
- [5] C. F. Hirjibehedin, C.-Y. Lin, A. F. Otte, M. Ternes, C. P. Lutz, B. A. Jones, and A. J. Heinrich, *Science* **317**, 1199 (2007).
- [6] N. Tsukahara, K. I. Noto, M. Ohara, S. Shiraki, N. Takagi, Y. Takata, J. Miyawaki, M. Taguchi, A. Chainani, S. Shin, and M. Kawai, *Phys. Rev. Lett.* **102**, 167203 (2009).
- [7] T. Balashov, T. Schuh, A. F. Takács, A. Ernst, S. Ostanin, J. Henk, I. Mertig, P. Bruno, T. Miyamachi, S. Suga, and W. Wulfhekel, *Phys. Rev. Lett.* **102**, 257203 (2009).
- [8] C. F. Hirjibehedin, C. P. Lutz, and A. J. Heinrich, *Science* **312**, 1021 (2006).
- [9] X. Chen, Y.-S. Fu, S.-H. Ji, T. Zhang, P. Cheng, X.-C. Ma, X.-L. Zou, W.-H. Duan, J.-F. Jia, and Q.-K. Xue, *Phys. Rev. Lett.* **101**, 197208 (2008).
- [10] L. Zhou, J. Wiebe, S. Lounis, E. Vedmedenko, F. Meier, S. Bluegel, P. H. Dederichs, and R. Wiesendanger, *Nat. Phys.* **6**, 187 (2010).
- [11] P. Wahl, P. Simon, L. Diekhöner, V. S. Stepanyuk, P. Bruno, M. A. Schneider, and K. Kern, *Phys. Rev. Lett.* **98**, 056601 (2007).
- [12] A. A. Khajetoorians, J. Wiebe, B. Chilian, S. Lounis, S. Blügel, and R. Wiesendanger, *Nat. Phys.* **8**, 497 (2012).
- [13] A. F. Otte, M. Ternes, S. Loth, C. P. Lutz, C. F. Hirjibehedin, and A. J. Heinrich, *Phys. Rev. Lett.* **103**, 107203 (2009).
- [14] A. F. Otte, Ph.D. thesis, Leiden University, 2008.
- [15] S. Loth, S. Baumann, C. P. Lutz, D. M. Eigler, and A. J. Heinrich, *Science* **335**, 196 (2012).
- [16] A. A. Khajetoorians, B. Baxevanis, C. Hubner, T. Schlenk, S. Krause, T. O. Wehling, S. Lounis, A. Lichtenstein, D. Pfannkuche, J. Wiebe, and R. Wiesendanger, *Science* **339**, 55 (2013).
- [17] J. Fernández-Rossier, *Phys. Rev. Lett.* **102**, 256802 (2009).
- [18] D. Dai, H. Xiang, and M. Whangbo, *J. Comput. Chem.* **29**, 2187 (2008).
- [19] M. H. L. Pryce, *Proc. Phys. Soc. London Sect. A* **63**, 25 (1950).
- [20] T. Schuh, T. Balashov, T. Miyamachi, S.-Y. Wu, C.-C. Kuo, A. Ernst, J. Henk, and W. Wulfhekel, *Phys. Rev. B* **84**, 104401 (2011).
- [21] S. Loth, C. P. Lutz, and A. J. Heinrich, *New J. Phys.* **12**, 125021 (2010).
- [22] See Supplemental Material at <http://link.aps.org/supplemental/10.1103/PhysRevLett.111.127203> for experimental details and additional information about the model.
- [23] The calculated N–Fe–N angle varies between models from 130° [5] to 175° [24].
- [24] J. Nicklas, A. Wadehra, and J. Wilkins, *J. Appl. Phys.* **110**, 123915 (2011).
- [25] F. A. Cotton, *Chemical Applications of Group Theory* (Wiley-Interscience, New York, 1990), 3rd ed.
- [26] We found no correlation between the variation in anisotropy and the distance of each dimer from the edge of the Cu<sub>2</sub>N island, or with the size of the islands. All dimers were more than 1 nm from the edge of the island.
- [27] S. ya Ohno, K. Yagyuu, K. Nakatsuji, and F. Komori, *Surf. Sci.* **547**, L871 (2003).
- [28] C.-Y. Lin, J.-L. Li, Y.-H. Hsieh, K.-L. Ou, and B. A. Jones, *Phys. Rev. X* **2**, 021012 (2012).